Talanta 85 (2011) 850–858

Contents lists available at ScienceDirect

Talanta

journal homepage: www.elsevier.com/locate/talanta

Very low optical absorptions and analyte concentrations in water measured by Optimized Thermal Lens Spectrometry

R.A. Cruz [a], M.C. Filadelpho [b], M.P.P. Castro [b], A.A. Andrade [c], C.M.M. Souza [d], T. Catunda [a,*]

[a] Institute of Physics of São Carlos, University of São Paulo, São Carlos, C.P. 369, Brazil
[b] Laboratório de Ciências Físicas/CCT, Universidade Estadual do Norte Fluminense – UENF, 28013-602 Campos dos Goytacazes, RJ, Brazil
[c] Instituto de Física, Universidade Federal de Uberlândia, UFU, C.P. 593, CEP 38400-902, Uberlândia, MG, Brazil
[d] Laboratório de Ciências Ambientais/LCA, Universidade Estadual do Norte Fluminense – UENF, 28013-602 Campos dos Goytacazes, RJ, Brazil

ARTICLE INFO

Article history:
Received 28 January 2011
Received in revised form 5 April 2011
Accepted 6 April 2011
Available online 8 May 2011

Keywords:
Thermal Lens Spectrometry
Water
Chromium(III)
Absorption spectrum
High sensitivity

ABSTRACT

Thermal Lens Spectrometry has traditionally been carried out in the single-beam and the mode-mismatched dual-beam configurations. Recently, a much more sensitive dual-beam TL setup was developed, where the probe beam is expanded and collimated. This feature optimizes Thermal Lens (TL) signal and allows the use of thicker samples, further improving the sensitivity. In this paper, we have made comparisons between the conventional and optimized TL configurations, and presented applications such as measurements of very low absorptions and concentrations in water and Cr(III) aqueous solution in the UV–vis range. For pure water we found linear absorption coefficients as low as the Raman scattering one due to the stretching vibrational modes of OH group. The detection limit was estimated 1×10^{-6} cm^{-1} with a 180-mW excitation power using a 100-mm cell length. This sensitivity is very high, considering that water has a photothermal enhancement factor ~33 times smaller than CCl_4, for example. For Cr(III) species in aqueous solution, the limit of detection (LOD) was estimated in ~40 ng mL^{-1} at 514 nm, or ~10 ng mL^{-1} at 405 nm, which is ~30 times smaller than the LOD achieved with conventional transmission techniques. The more recent TL configuration is very attractive to obtain absorption spectra, since the result does not depend critically on the beam parameters, unlike the other configurations. The main drawbacks of this optimized TL configuration are the longer acquisition time and the need for larger samples.

1. Introduction

Thermal Lens Spectrometry (TLS) [1–10] belongs to a family of photothermal techniques of high sensitivity used to measure spectroscopic and thermo-optical properties of materials. Other techniques belonging to this class are photoacoustic spectroscopy (PAS) [11], photothermal interferometry, photothermal deflection (PTD) [12], and laser calorimetry (LC) [13]. Photothermal techniques are sensitive to the heat generated by non-radiative relaxation processes after absorption of radiation. These methods are considered indirect ways of measuring the optical absorption, since in fact they measure the effect produced by absorption. They are ~3 orders of magnitude more sensitive than conventional transmission methods and are inherently insensitive to scattering and reflection losses, which usually limit the sensitivity of transmission techniques.

The TL experiment can be carried out with a single beam (SB) [14], where the same beam excites the sample and probes the effect, or with dual beam, where one beam excites the sample and the other probes it [15]. In the first case, the sample is usually placed at about one Rayleigh range from the focus. In the second one, in general both beams are focused and their waists are displaced from each other, which is named mode-mismatched dual-beam TL configuration. The term mode-matched is used when the sample is located at the confocal position of both excitation and probe beams, and the radii of these two beams are nearly the same. Fang and Swofford highlighted that larger sensitivity is achieved by varying the distance between the beam waists [7], as verified by Berthoud et al. [16] through a systematic study on the geometry of dual-beam configurations. In fact, the mode-mismatched setup is more sensitive with the probe beam diameter larger than the excitation one, so that it covers a larger part of the temperature profile. Sheldon et al. [14], and Shen et al. [17] developed a quantitative model for the TLS, using the diffraction integral approach.

Recently, Marcano et al. performed the TL experiment in a new dual-beam configuration [18], where the excitation beam is focused on the sample and the probe one is expanded (to ~1 cm diameter)

* Corresponding author.
E-mail address: tomaz@ifsc.usp.br (T. Catunda).

0039-9140/$ – see front matter © 2011 Published by Elsevier B.V.
doi:10.1016/j.talanta.2011.04.015

and highly collimated. In this case, the effective area of the probe beam is 4 orders of magnitude larger than the excitation beam. In this configuration, the stationary TL signal becomes independent of the Rayleigh parameters of excitation and probe beams. This feature not only strongly simplifies the experimental procedure but also improves the measurement accuracy, since beam waists and their positions no longer need to be precisely determined because the TL signal does not depend critically on these parameters. Furthermore, this configuration presents a single peaked *Z*-scan signal, with a broad maximum which allows the use of thick samples, further improving the sensitivity. Although the excitation and probe beams in Marcano et al.'s TL configuration are nearly confocal [18], it was named mode-mismatched because the waist of the probe beam is much larger than the excitation's. In this paper, we named this configuration as optimized mode-mismatched (OMM) in order to distinguish it from the most traditionally used, named here as conventional mode-mismatched (CMM) dual-beam TL configuration.

The OMM approach was recently applied to the study of low absorptions ($\sim 10^{-2}\ m^{-1}$) in organic liquids [19]. More recently, we published a letter with very low absorption measurements in blue-UV region in pure water [20]. Using a 100-mm cell length, absorption of $1.5 \times 10^{-3}\ m^{-1}$ was found at 364 nm, which is the lowest value ever obtained for water. The sensitivity was of $10^{-4}\ m^{-1}$ for a ~180-mW excitation power, which is somehow surprising because water is known as a bad liquid for photothermal spectrometry due to the small value of its photothermal enhance factor (~33 times lower than CCl_4) [21].

Information on the water's absorption spectrum in the UV-blue is an experimental challenge which has been receiving prior attention due to its importance to many fundamental and applied disciplines [22–29], such as remote sensing of natural waters, phytoplankton productivity, aquatic photochemistry, etc. Several groups have studied the water's spectrum using different techniques: Conventional Transmission, Integrating Cavity (IC), PTD, PAS, LC, and TLS [11,12,20,22–24]. It is well known that water has a transparent window in the visible, where its absorption drops by 8 orders of magnitude compared to IR and UV. It is particularly transparent between 300 and 450 nm where the absorption determination is an experimental challenge. The discrepancy between literature results has been attributed mainly to sensitivity limitations and water quality. In fact, "pure water" is an idealization and the role of purification system has been subject of debate between different research groups [25,26]. According to Morel et al.'s [27], 'it is common practice to believe that the lowest absorption values are the best ones, as a consequence of a better purification'.

Most of the results in water were obtained by some variation of the transmission technique, which is not sensitive enough to determine absorptions lower than $0.01\ m^{-1}$, even with the use of long cells (up to 5 m) [28]. For example, the results from Litjens et al. present uncertainty $\pm 2.6 \times 10^{-2}\ m^{-1}$ (at 360 nm) [29], which is one order of magnitude larger than the lowest absorption obtained by TL [20]. In addition transmission techniques require corrections due to molecular and particle scatterings, which is always cumbersome. Photothermal techniques are intrinsically insensitive to scattering and are appropriate for ultrasensitive spectroscopy. Tam and Patel have used PAS [11] and obtained relatively high absorption values (minimum of $\sim 2 \times 10^{-2}\ m^{-1}$ at 480 nm) compared to more recent results using PTD [12] and IC [22]. This discrepancy has been attributed to water quality [22]. The PTD measurements were significantly important since the authors obtained a minimum absorption of $(6.2 \pm 0.6) \times 10^{-3}\ m^{-1}$ at ~420 nm, with a 10% uncertainty (more than one order of magnitude lower than the detection limit of conventional transmission measurements). These results were corroborated by IC measurements performed in the same group, led by Fry. More recently, Morel et al. carried out hyperspectral irradiance measurements in natural waters [27], concluding that the absorption in pure water should be smaller than the results of Fry's group below 420 nm. In our previous study [20], the minimum absorption, around 380 nm, is lower than that in all literature results, in agreement with Morel et al.'s conclusions. Above 420 nm, our spectrum agrees with Fry group's. Although TLS and PTD are conceptually similar, the calibration of PDS is extremely difficult [26]. On the other hand, in principle the OMM TL configuration needs no calibration, since the signal does not depend critically on the beam parameters (unlike other TL configurations).

In the present paper, we provide details on use of the OMM TL configuration in pure water, tap water and Cr(III) solutions. A comparison between the OMM, CMM, and SB configurations is presented using theoretical and experimental data. The effect of Rayleigh and Raman scattering was analyzed on the absorption spectrum of the purified water. By combining the OMM TL and conventional transmission techniques, we also studied light scattering in tap water. In the measurements of Cr(III) species in HCl (1 N) aqueous solution, the limit of detection (LOD) was estimated 40 ng mL^{-1} at 514 nm, or 10 ng mL^{-1} at 405 nm, which corresponds to nearly one order of magnitude smaller than the maximum limit level for natural and drinking waters [30].

2. Experimental

2.1. Calculation of the thermal lens signal

The TL effect is induced when a laser beam passes through the sample and the absorbed energy is converted into heat. The consequent change in the refractive index, provoked by a temperature rise, produces a lens-like optical element into the sample, since the refractive index depends on temperature according to $n(T) = n_o + (dn/dT)\Delta T$. The propagation of the beam then will be affected resulting in the spreading or focusing of the beam depending on the sign of the temperature coefficient of refractive index, dn/dT. The thermally induced nonlinear refraction causes the wave front to curve, which produces a transversal phase shift. By measuring the intensity change at the beam center, the thermo-optical properties of the sample can be determined. Fig. 1(a) shows a typical configuration for the CMM dual-beam experiment. In the sketch, w_{op} and w_{oe} are respectively the probe and excitation beam waist radii, and w_p is the probe beam radius at the sample (the excitation beam radius at the sample is $w_e = w_{oe}$). Z and Z_2 correspond respectively to the positions of the sample and the aperture with regard to the probe beam waist (assumed to be at $Z = 0$). The Gaussian beam waist is expressed by $w(z)^2 = w_0^2[1 + (Z/Z_c)]$, where $Z_c = \pi w_o^2/\lambda$ is the Rayleigh range (or confocal parameter), and λ is the beam wavelength (for the excitation beam, the notation is Z_{ce} and λ_e, and for the probe beam, Z_{cp} and λ_p). Using the Fresnel's diffraction integral, the TL signal for low absorptions ($\theta \ll 1$) is given by [17]:

$$S(Z,t) = \frac{I(t) - I_0}{I_0} = -\theta\,\mathrm{ArcTan}\left(\frac{2mV}{[(1+2m)^2 + V^2](t_c/2t) + 1 + 2m + V^2}\right) = -\theta\mathrm{ArcTan}[f(Z,t)] \quad (1)$$

where I_0 is the on-axis intensity when t is zero, $m = (w_p/w_e)^2$, and

$$V = \frac{Z}{Z_{cp}} + \frac{Z_{cp}}{Z_2 - Z}\left[1 + \left(\frac{Z}{Z_{cp}}\right)^2\right] \quad (2)$$

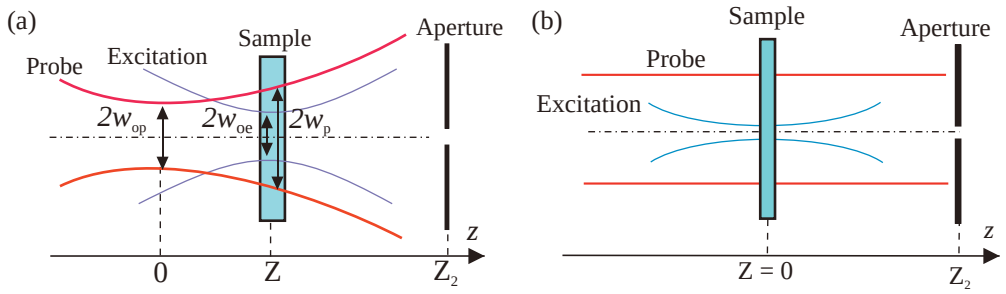

Fig. 1. (a) Typical beam configuration for the conventional mode-mismatched (CMM) TL experiment. Both beams are focused, and the sample is placed at the excitation beam waist. (b) Optimized mode-mismatched (OMM) TL configuration, where the excitation beam is focused and the probe one is expanded and collimated.

The characteristic heat diffusion time (or TL characteristic time) is:

$$t_c = \frac{{w_e}^2}{4D}, \tag{3}$$

where $D = k/\rho C_p$ is the thermal diffusivity, k is the thermal conductivity, ρ is the density, and C_p is the specific heat. The amplitude of the induced phase shift is:

$$\theta = -P_e a l \varphi \frac{dn/dT}{\lambda_p k} = -Eal\varphi \tag{4}$$

P_e, a, l, and φ are respectively the excitation beam power, the linear optical absorption coefficient, the sample thickness, and the fraction of absorbed energy converted into heat. Eq. (4) also defines the Photothermal Enhancement Factor, $E = P_e(dn/dT)/(\lambda_p k)$, which is the ratio between the TL signal and the conventional transmission signal [31]. The SB set-up can be also described by Eq. (1) considering that $m = 1$ [14]. By fitting the transient TL signal with Eq. (1), the parameters θ and t_c can be obtained, which in turn can provide the linear absorption coefficient (a) and the thermal diffusivity (D).

The OMM configuration uses a focused excitation beam and an expanded and highly collimated probe one [18], with both beam waists and the sample at the same position ($Z = 0$), as sketched in Fig. 1(b). Typically $Z_2 \sim 150$ cm and the probe beam diameter is ~1 cm, resulting in $Z_{cp} \sim 10^4$ cm, so $Z_{cp} \gg Z_2 \gg Z_{ce}$. The probe beam is nearly constant in Fig. 1(b) due to the very large value of Z_{cp}. It is important to note that in OMM, the detector is in the near field ($Z_2 \ll Z_{cp}$) as opposed to the cases of SB and CMM, which works in far field. This distinction is related to the parameter V (Eq. (2)) that assumes very different values in the OMM ($V \sim Z_{cp}/Z_2$) and CMM ($V \sim Z/Z_{cp}$) configurations. The distinction between near and far field conditions can also be expressed by the effective Fresnel number of Gaussian beam, $N_F = 4Z_{cp}/\pi Z_2 \sim 1.27 Z_{cp}/Z_2$. Consequently, $N_F \ll 1$ for far field condition ($Z_2 \gg Z_{cp}$) and $N_F \gg 1$ for near field.

Fig. 2 presents a comparison of the Z dependence of the TL signal for the SB (dotted line), CMM (dashed line), and OMM (solid line) TL configurations. All curves were obtained by Eq. (1). The origin of the graph ($Z = 0$) is defined at the probe beam waist. For the SB configuration, the signal $S(Z)$ is an odd function with symmetric peak and valley positions, $Z = \pm\sqrt{3}Z_c$ (or $V = \pm\sqrt{3}$) and the maximum signal amplitude is $S_{max} = 0.52\theta$. The CMM situation was simulated considering the excitation beam waist fixed at $Z = 5$ cm, where the

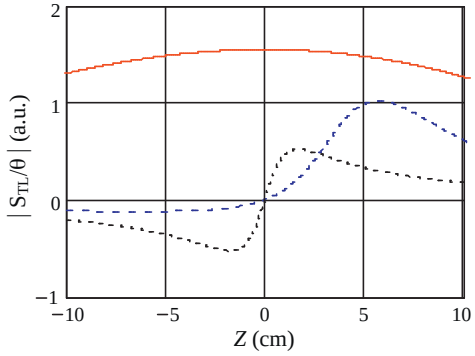

Fig. 2. Comparison between TL signals [$f(Z,t)$ in Eq. (1)] as a function of the sample position, Z, calculated for the OMM (solid line), the CMM (dashed line), and the SB (dotted line) configurations. The origin $Z = 0$ is defined at the probe beam waist. Common parameters: $\lambda_e = 514$ nm, $w_{oe} = 40.5$ μm ($Z_{ce} = 1$ cm), $\lambda_p = 632.8$ nm, and $Z_2 = 150$ m. For SB: $\lambda = 514$ nm.

signal (as well as the parameter m) is close to its maximum value (at $Z \sim 5.7$ cm). For the OMM configuration, the signal presents a symmetric broad maximum ($|S_{max}/\theta| \cong 1.57$ at $Z = 0$), which allows the use of thick samples. This feature is important to improve the sensitivity since TL signal increases linearly with the sample length (Eq. (4)). The parameters used in Fig. 2 are summarized in Table 1, and correspond to typical values for each configuration. In this table, the Z value corresponds to the position of the sample in the TL experiment, which coincides with the excitation beam waist (except in the SB case, where the sample is positioned at $Z = \pm\sqrt{3}Z_c$).

In Eq. (1), $S(Z,t)$ is proportional to the ArcTan[$f(Z,t)$] function, with reaches the asymptotic maximum $\pi/2 \cong 1.57$ for $f \to \infty$. Since $m \gg V$ in the OMM configuration, the function becomes $f(Z = 0, t \to \infty) \sim 2\,\text{mV}/(2m + V^2) \sim V$ (considering only the order of magnitude). For $V = 70$ (Table 1), for example, ArcTan(70) ≅ 1.56. Therefore in the OMM configuration [18]:

$$S = \frac{I_\infty - I_0}{I_0} \cong -\frac{\pi}{2}\theta \cong -1.57\,\theta, \tag{5}$$

where I_∞ is the on-axis intensity at the steady-state ($t \to \infty$, or $t \gg t_c$). It should be noticed that Eq. (5) does not depend on parameters V and m, unlike Eq. (1). This is an advantage of OMM over CMM and SB configurations. In these cases, the values of the probe and

Table 1
Typical values of TL parameters in different configurations: Z, sample's position in the TL experiment; Z_{cp}, probe beam confocal (Rayleigh) parameter; w_{op}, probe beam waist radius; $m = (w_{op}/w_{oe})^2$, ratio of the beam areas of probe and excitation; V, parameter from Eq. (2); t_R/t_c, normalized TL rise time; N_F, Fresnel number; and $f(Z,t \to \infty)$, TL signal amplitude. Common parameters: $Z_{ce} = 1$ cm, $\lambda_p = 632.8$ nm, and $\lambda_e = 514$ nm (for SB, $\lambda_p = \lambda_e = 514$ nm).

	Z (cm)	Z_{cp} (cm)	w_{op} (mm)	$V(Z)$	$m(Z)$	t_R/t_c	N_F	$f(Z,t \to \infty)$
SB	1.73	1	~0.04	$\sim Z/Z_{cp} = \sqrt{3}$	1	7.5	0.008	~0.52
CMM	5	3	~0.08	$\sim Z/Z_{cp} \sim 2$	~14	100	0.03	~1.0
OMM	0	10,000	~4.5	$\sim Z_{cp}/Z_2 \sim 70$	~12,300	1100	85	~1.56

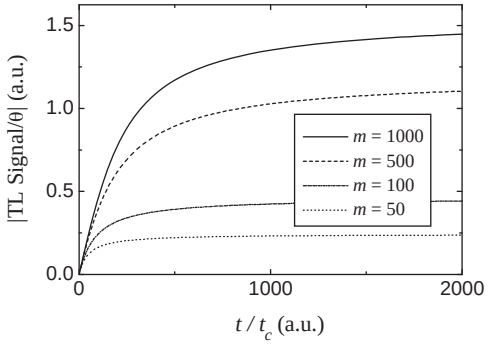

Fig. 3. Transient TL signals calculated by Eq. (1) for different values of $m=(w_p/w_e)^2$. Parameters: $\lambda_e=\lambda_p=500$ nm, $Z_{ce}=1$ cm (or $w_{oe}\cong 40$ μm), $Z=0$, $Z_2=1.5$ m, and $m=50$, 100, 500, and 10,000 (which correspond to $Z_{cp}=0.5$, 1, 5, and 100 m, respectively).

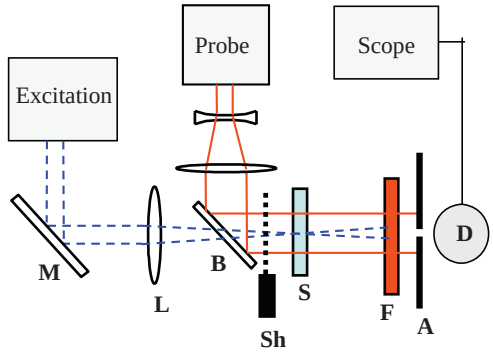

Fig. 5. OMM TL experimental setup: the excitation beam is focused into the sample, and the probe one is expanded and collimated. M, mirror; L, lens; B, beam splitter; Sh, shutter; S, sample; F, filter; A, aperture; D, detector.

excitation beam waists and their positions relative to the sample have to be carefully measured, which is cumbersome and contributes for the increase of the experimental uncertainty [14,17]. This problem is particularly important when several excitation lasers are used in order to cover a wide spectral range, as in this study.

Fig. 3 refers to transient TL signals obtained using Eq. (1) for different values of $m=(w_p/w_e)^2$, which is the ratio of the effective beam areas. It shows that the rise time of the TL signal does not depend only on t_c but also increases with the parameter m. For a given value of t_c and w_{oe} (or Z_{ce}), it takes much longer for the transient signal to reach stationary state as m (or Z_{cp}) increases. This occurs because it takes longer for the heat to diffuse to the whole profile of the probe beam. In order to better describe this behavior, we define an effective rise time parameter (t_R) as the time necessary for the TL signal to reach 90% of its steady-state value. Fig. 4 shows the increase of t_R with the parameter m, which is linear up to $m\sim 30$ and reaches a plateau at $m\sim 2000$.

2.2. Thermal Lens setup

In the OMM experimental setup, showed in Fig. 5, the excitation beam was focused into the sample by a lens (L) of 20-cm focal length. In order to cover the spectral range from 351 to 528 nm, different lasers were used as excitation beam: Ar^+ (351, 364, 457, 476, 488, 496, 501, 514, and 528 nm), Kr^+ (413 and 406 nm), or He–Cd (442 nm). The probe beam, a He–Ne laser at 632.8 nm, was expanded and collimated generating a beam with a diameter of ~9.8 mm, which was aligned with the excitation beam by means of a glass beam splitter of ~1 mm length (*B*). Two kinds of cell were employed: a commercial quartz cell (Sigma, QS-1000) with a 9.5-cm length, and another made of Teflon with quartz windows, with a 30-mm diameter and variable length (5–100 mm). A dichroic filter (*F*) transmitted only the probe beam, which fell on aperture (*A*) with diameter of either 200 μm or 1 mm put in front of a Thorlabs' DET310 photo-detector (*D*). The signal was recorded in a Tektronix's TDS210 digital oscilloscope. To modulate the excitation power, a shutter (Sh) was utilized. However, unlike Marcano et al.'s experiment [18], the shutter was placed between the beam splitter and the sample, because the thermal expansion of the beam splitter can affect the measured signal when high sensitivity is required. For example, it causes an effect ~8 times larger than the TL signal for a pure water sample at 364 nm. With the modification above cited, the beam splitter's expansion does not present a transient behavior, and consequently does not affect the TL signal. For the same reason, no mirror was put between the sample and the detector. Instead, the aperture was placed straight forward the beam leaving the sample, at a distance $Z_2\cong 1.3$ m from the sample. The filter was set close the aperture, so that eventual TL effects on the filter does not affect the measurement. To prove it, the shutter was placed after the sample and no signal was observed.

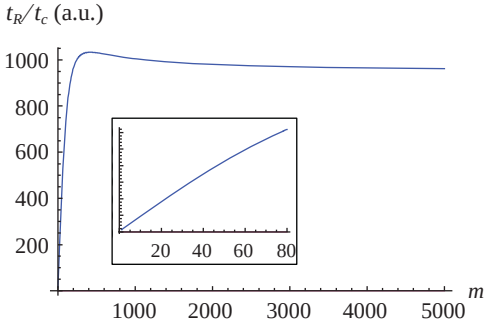

Fig. 4. The rise time parameter (t_R) of the TL signal [defined as the time to reach 90% of the steady-state signal from Eq. (1)] plotted as a function of the parameter m. The inset shows the linear behavior up to $m\sim 30$.

Another difference between this experimental setup and Marcano et al.'s [18] is the aperture with 1 mm diameter instead of 100 μm, in order to obtain a larger signal-to-noise ratio. This procedure reduces the TL signal amplitude, particularly in the OMM configuration. That is because the detection is made in the near field and consequently the TL effect is concentrated close to the center of the beam. Measurements of the dependence of the TL signal with aperture diameter showed that, for $Z_2\cong 125$ cm, a 1-mm aperture reduces the signal by approximately 38% compared to the 100-μm aperture. This can be also theoretically calculated using the diffraction integral [32]. Therefore, this effect was introduced as a calibration factor in θ calculation. On the other hand, the parameter t_c obtained by the fitting of the transient signal practically is not altered by this increase in aperture.

In the CMM configuration, both the excitation and the probe beams are focused by convergent lenses of ~20-cm focal length. The beams cross each other at a very small angle (<2°), and their waists are slightly separated from each other. The sample, placed in a quartz cuvette with a 2.0-mm length, is positioned at the excitation beam waist. The measurements of the beam waists were carried out with an Omega Meter Beam Profiler from Thorlabs Inc. More information about the CMM configuration can be found elsewhere [17].

Fig. 6 presents two typical transient TL signals obtained in the CMM (Fig. 6a) and OMM (Fig. 6b) configurations for pure water excited at 514 nm. In OMM, the transient took about 5 s to reach the steady-state, that is, 3 orders of magnitude longer than the TL characteristic time ($t_c\sim 3$ ms). At $Z\approx 0$, the excitation beam waist ($w_e\cong 38$ μm) is ~130 times smaller than the probe

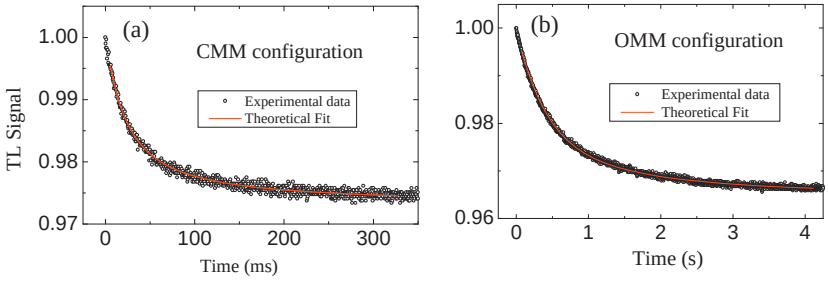

Fig. 6. Comparison between transient TL signals obtained with two different configuration for pure water at 514 nm: (a) CMM configuration (l = 2 mm, P_e = 1.4 W, $w_{oe} \cong 42.3$ μm); fitting parameters: V = 1.9; m = 18; fitting result: $\theta = 0.0263 \pm 0.0002$ rad, and $t_c = 2.77 \pm 0.04$ ms (R = 0.987, n = 16, P = 0.95); (b) OMM configuration using a 1 mm aperture (l = 9.5 mm, $P_e \cong 392$ mW, $w_{oe} \cong 38$ μm); fitting parameters: V = 95.5; m = 16627; fitting result: $\theta = 0.0226 \pm 0.0006$ rad, and $t_c = 2.56 \pm 0.01$ ms (R = 0.9994, n = 10, P = 0.95). Both fits were made with Eq. (1).

beam one, resulting in the parameters $m = (w_{op}/w_{oe})^2 \cong 16{,}630$, and $V(Z) = Z_{cp}/Z_2 \cong 96$. The fit of Fig. 6's data by Eq. (1) provides the parameters t_c and θ, by which thermal diffusivity and optical absorption can be found (by Eqs. (3) and (4), respectively). However, in OMM, we usually determine θ from the stationary value of the TL signal by Eq. (5). In order to improve the data statistics, TL measurements usually are performed as a function of P_e, so that the parameter θ/P_e is obtained from the linear plot of θ vs P_e. When very high sensitivity is required, the quality of the sample or the cell windows also contributes for the experimental uncertainty. Therefore, measurements were replicated several times, using always a fresh sample. At λ_e = 514 nm, for example, we obtained the absorption coefficients $a = 0.036 \pm 0.004\ \mathrm{m^{-1}}$ (mean ± SD; n = 5) in CMM, and $a = 0.034 \pm 0.003\ \mathrm{m^{-1}}$ (mean ± SD; n = 6) in OMM. Considering the experimental uncertainty, these results agree with each other and with the literature [22]. This agreement also was observed at 528 nm, whose results were $a = 0.041 \pm 0.004\ \mathrm{m^{-1}}$ in CMM and $a = 0.040 \pm 0.004\ \mathrm{m^{-1}}$ in OMM. All results for water were calculated using the literature data: k = 0.60 W/m K and $dn/dT \cong -98 \times 10^{-6}\ \mathrm{K^{-1}}$ (at 632.8 nm) [33]. The thermal diffusivity calculated from the parameter t_c obtained also from the transient fit is (Eq. (3)): $D = (1.6 \pm 0.3) \times 10^{-3}\ \mathrm{cm^2/s}$ in CMM, and $(1.4 \pm 0.2) \times 10^{-3}\ \mathrm{cm^2/s}$ in OMM. Taking into account the uncertainty, the results agree with literature value, $1.44 \times 10^{-3}\ \mathrm{cm^2/s}$ [34]. The same D value was found for tap water using the TL OMM configuration.

One important advantage of the OMM configuration is the possibility of the use of long cells, in order to improve the sensitivity. However, for $l \gg Z_{ce}$, the excitation beam diameter, and consequently the parameter $m = (w_{op}/w_{oe})^2$, vary along the cell, decreasing the TL signal (Fig. 2). We theoretically simulated this effect by integrating the signal along the sample length and verified a reduction smaller than 1.5% for l = 100 mm, which is much smaller than the experimental uncertainty of ~10%. It is important to notice that the relation $Z_{cp} \gg L \gg Z_{ce}$ remains valid along the sample. Experiments with several cells were performed to investigate the dependence on the cell length, varying l from 5 to 100 mm. Fig. 7 shows a linear increase of the TL signal (n = 6, R = 0.9999, P = 0.95) as theoretically expected. Thus, the use of a 100-mm cell represents an enhancement of about two orders of magnitude in the experimental sensitivity compared with most of TL set-ups where $l \sim 1$ mm is used. However, for $l < 5$ mm, a departure from this linear behavior was observed, and the signal amplitude is smaller than expected. We believe that this behavior is due to the effect of axial heat flow, similarly to the effect studied by Shen et al. in thin films [35]. Since the effective response time of the TL signal in the OMM configuration is much longer than in the SB and CMM ones, the OMM should be more sensitive to axial heat flow.

The OMM technique's sensitivity was estimated at $\sim 2 \times 10^{-5}\ \mathrm{m^{-1}}$ for water, and $\sim 6 \times 10^{-7}\ \mathrm{m^{-1}}$ for CCl_4 (with P_e = 1 W) [20]. This later value corresponds to a temperature change $\Delta T \sim 2P_e a/\pi k \sim 10^{-7}$ °C [36], or a refraction index change $\Delta n = (dn/dT)\Delta T \sim 10^{-11}$.

All the measurements were performed at room temperature (~295 °C).

2.3. Sample preparation

The water samples were purified by means of two successive commercial purification systems: in the first one, the water was deionized and filtered by Reverse Osmosis (GEHAKA); in the second, it was purified by a Millipore's Milli-Q Plus Ultrapure Water System. The resistivity of the final sample was 18.3 MΩ cm. This whole system is constantly used, allowing a short lifetime of the water in the reservoir, which avoids contamination. Measurements were carried out many times in several days, in order to verify the reproducibility. The sample was often changed by a fresh one.

To remove any organic impurity from the cells, they were immersed in a solution of water, $K_2Cr_2O_7$, and H_2SO_4 for about 15 min. Next, they were copiously rinsed subsequently with tap, bidistilled, and purified water. Then, in order to avoid mark on the windows, the cells were immediately filled with purified water. This latter procedure is as important as the sample purification, since stains on the windows can absorb even more than the sample, as we have observed.

The Cr(III) aqueous solutions were prepared with Merck Suprapur Hydrochloric acid, doubly distilled water, and Merck's standard solution (1 mg mL^{-1}). All other chemicals were of analytical reagent grade. Cr(III) working solutions in the range between 0.1 and 25 mg L^{-1} were obtained by proper dilution. The HCl concentra-

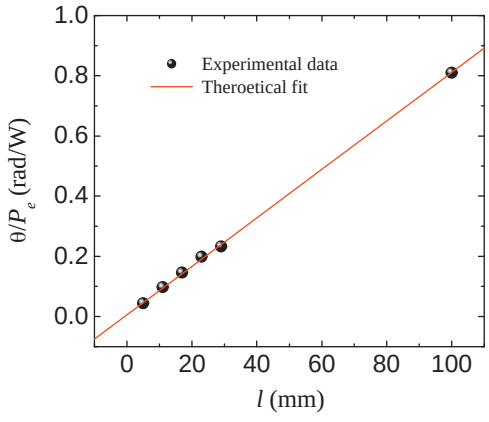

Fig. 7. TL signal amplitude (for pure water) as a function of the cell length, measured in the OMM configuration. The graph shows a linear increase of the signal as theoretically expected (n = 6, R = 0.99985). Experimental parameters: λ_e = 514 nm, $w_{oe} \cong 38$ μm, λ_p = 632.8 nm, $w_{op} \cong 4.9$ mm.

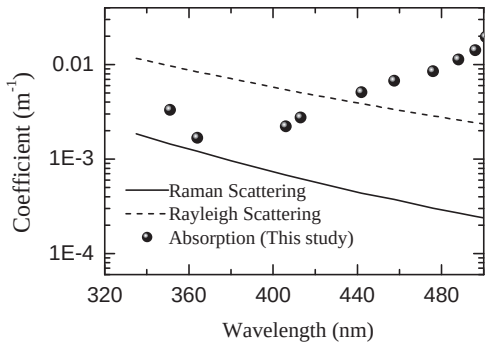

Fig. 8. Comparison between the linear absorption coefficient measured in the OMM TL configuration (our results) and theoretical values of Raman [37] and Rayleigh [29] scatterings, for pure water.

tion in the samples was of 4.2% (1 N) to keep the oxidation state of Cr(III).

3. Results and discussions

3.1. Low optical absorption – water

Pure water has very small absorption ($<10^{-2}$ m^{-1}) in the UV-blue spectral region; it is relatively stable under laser excitation (nondegradable), and its enhancement factor (Eq. (4)) is one order of magnitude smaller than typical organic solvents. Therefore, it is a good medium to test and optimize high-sensitivity TL absorption measurements.

Our spectrum indicates a minimum absorption value lower than 2×10^{-3} m^{-1}, between 360 and 400 nm (Fig. 8), which is about one order of magnitude smaller than the estimated value of Rayleigh (elastic) scattering [29], and comparable to Raman (inelastic) scattering due to the stretching vibrational modes of OH group [37]. TL technique is not sensitive to elastic scattering, but in the inelastic case, a fraction of scattered energy is converted into heat, which contributes to the TL effect. For example, at 380 nm (~26,300 cm^{-1}) this fraction is ~13%, considering the 3400 cm^{-1} Raman shift. Because we are interested only in the absorption coefficient, not in the scattering one, we should subtract this percentage from the TL signal. In fact, this reduction (~10%) is smaller than the experimental error (~40%) in the UV region, where this effect is larger. Using an Ocean Optics USB2000 spectrometer with resolution of 1.3 nm, the scattering was observed at the direction perpendicular to the incident beam, for several excitation wavelengths. The vibrational Raman shift was the same (~3400 cm^{-1}) for all excitation wavelengths, as expected. Fig. 9 shows the scattered light spectra in pure water at two excitation wavelengths, 351 and 364 nm. The Rayleigh intensity was about one order of magnitude larger than the Raman one, which agrees with the estimated values of the literature shown in Fig. 8.

Transmission techniques determine the attenuation coefficient, $c(\lambda) = a(\lambda) + b(\lambda)$, where a and b account for absorption and scattering respectively. Thus, to obtain the correct value of absorption from a transmission measurement, scattering losses and the uncertainty in cuvette reflections should be known, which limits the efficacy of this method. Moreover, the scattering coefficient has two contributions, from molecules (b_m) and particulates (b_p), that is, $b(\lambda) = b_m(\lambda) + b_p(\lambda)$. Although the molecular scattering can be theoretically estimated, the particulate contribution remains unknown. TL spectrometry is not sensitive to scattering [38], since it is sensitive to heat only. Moreover, the TL signal is normalized by the initial intensity (I_o), according Eq. (5). Thus, the scattering and reflection losses affect I and I_o in the same way, so that the need for taking into account these effects is removed.

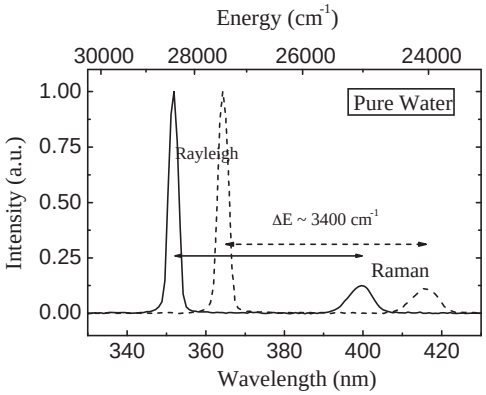

Fig. 9. Scattered light spectra in pure water under 351 nm (solid line) and 364 nm (dotted line) excitation. The Raman shift (~3400 cm^{-1}) is nearly independent on the excitation wavelength.

It is interesting to remark that the conventional transmission technique can complement the TL one in order to determine the scattering coefficient. As an example, we applied these two techniques for a tap water sample in the UV region (Fig. 10). The attenuation coefficient (c) could be determined by transmission measurements using the 100-mm cell; the absorption coefficient (a) was measured by TL, and the scattering one was calculated by subtracting the absorption from the attenuation. The result is about one order of magnitude larger than the estimated value for Rayleigh scattering of pure water. Therefore, it was associated to impurities in this tap water. To obtain the tap water's optical absorption, the same parameters k and dn/dT of pure water were used, since diffusivity values of tap and pure waters were approximately the same. Fig. 11 compares absorption spectra obtained by OMM for the pure and tap waters. Although the tap water absorption is similar to that of pure water above 457 nm, in the UV (335–364 nm), the tap water absorption is one order of magnitude larger. These results (Figs. 10 and 11) reveal that both absorption and scattering in water in the UV-Blue range are extremely sensitive to impurities, which could be the reason for the data discrepancy in the literature.

All of our results, for pure and tap waters, are summarized in Table 2.

3.2. Low concentration – Cr (III) aqueous solution

Although Cr(III) in small amounts is an important nutrient needed by the human bodies, swallowing large amounts of Cr(III) may also cause health problems, *e.g.*, lung cancer [39]. In plants,

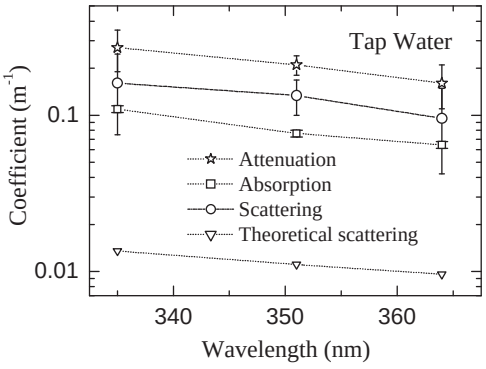

Fig. 10. Tap water results. Total attenuation coefficient (c) determined by conventional transmission technique (star); absorption coefficient (a) measured by OMM TL (square); scattering coefficient [$b(\lambda) = c(\lambda) - a(\lambda)$] calculated by subtracting the absorption from the attenuation (circle); theoretical Rayleigh scattering (triangle) [29].

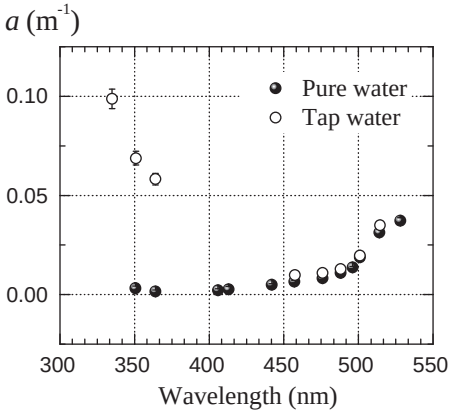

Fig. 11. Comparison between pure and tap waters. Linear absorption coefficient obtained by OMM TL configuration.

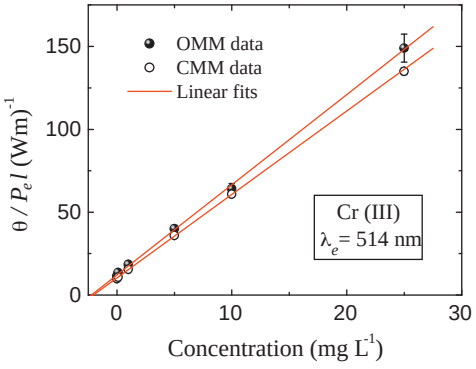

Fig. 12. Normalized TL signal ($\theta/P_e l$) versus chromium concentration in HCl (4.2%) aqueous solution, for OMM and CMM TL configurations.

toxic concentrations of Cr(III) usually promote chlorosis and necrosis of leaves as a consequence of photosynthesis inhibition and disturbance in mineral nutrition [40], which can eventually promote a decrease in the rates of plant growth [41]. Therefore, it is important to monitor theses inorganic elements with high sensitivity.

The TL measurements were performed as a function of the excitation power for each Cr concentration. In this case, a linear dependence between the TL signal and the excitation power was observed, which indicates the absence of any photochemical processes for Cr(III), in contrast with Pedreira et al.'s report on the Cr(VI)-diphenylcarbazide complex [10]. Fig. 12 shows the variation of $\theta/P_e l$ as the chromium concentration (c) increases, for the OMM and CMM TL configurations at 514 nm excitation. There is a good agreement between the two configurations up to ~10 mg L^{-1}. OMM presented a larger uncertainty due to the long time to reach the steady-state in this configuration, which makes it more sensitive to signal distortions owing to absorbing impurities in the sample. The fit of data ($n = 6$, $R = 0.99995$, and $P = 0.95$) from the CMM configuration provided the linear equation: $\theta/P_e l = (5.0 \pm 0.1)c + (10.4 \pm 0.2)$. The minimum detectable concentration change is determined by the uncertainty on the TL signal, which in this case is 0.2 rad/Wm. Thus, the limit of detection (LOD) is $\Delta X = 0.2/5.0 \cong 0.04$ mg L^{-1}, or 40 ng mL^{-1}, lower than the limit level (100 ng mL^{-1}) for natural and drinking waters [30]. It is important to note the difference between the LOD for low concentrations and detection limit for low absorptions. The latter depends on the photothermal enhancement factor of the solution and the sample length (as we have already discussed). The former is related to the minimum TL signal variation that can be detected. Thus, the way to reduce the LOD is improving the experimental precision. This could be reached by improving the sample quality (reducing the impurity degree), increasing either the excitation power or the sample length, or improving the electronic apparatus.

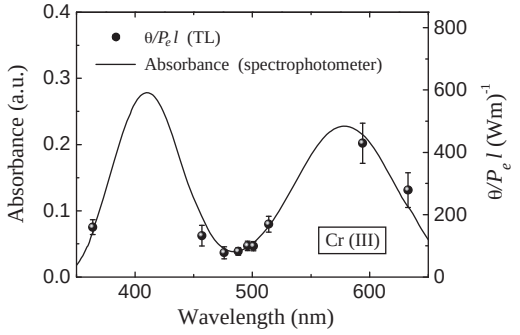

Fig. 13. Absorption spectrum of Cr(III) in HCl (4.2%) aqueous solution. Left axis: absorbance obtained by a SHIMADZU 1601PC spectrophotometer with $l = 10$ mm and $c = 1$ mg mL^{-1}; right axis: TL signal ($\theta/P_e l$) measured in the OMM configuration with $l = 10$ mm and $c = 25$ mg L^{-1}.

The LOD also depends on the ion absorption. Fig. 13 (solid line) shows the absorption spectrum of the Cr(III) solution obtained using a SHIMADZU 1601PC spectrophotometer. If the sample was pumped at ~405 nm, *e.g.*, where the absorption is 4 times larger than at 514 nm, the LOD would be 4 times lower, *i.e.*, 10 ng mL^{-1}. For example, the samples studied by Pedreira et al. (Cr(VI) complex) [10], have an absorption ~100 times larger (in 514 nm) than our sample, which corresponds to a LOD of ~0.4 ng mL^{-1} (ppb) (Pedreira et al. reach a little larger LOD due to their larger uncertainty).

Table 2
Absorption coefficients (a) for pure and tap waters (by OMM TL configuration), and attenuation coefficients (c) for tap water (by conventional transmission technique). Results from the present study (mean ± SD, $n = 6$).

λ_e (nm)	a (10^{-2} m^{-1}) pure water $l = 100$ mm	a (10^{-2} m^{-1}) pure water $l = 9.5$ mm	a (10^{-2} m^{-1}) tap water $l = 100$ mm	c (10^{-2} m^{-1}) tap water $l = 100$ mm
335	–	–	11.0 ± 0.5	27 ± 8
351	0.4 ± 0.1	0.3 ± 0.1	7.5 ± 0.3	21 ± 3
364	0.19 ± 0.09	–	6.3 ± 0.3	16 ± 5
406	0.24 ± 0.09	–	–	–
413	0.3 ± 0.2	–	–	–
442	0.54 ± 0.08	–	–	–
457	0.70 ± 0.08	0.6 ± 0.2	1.1 ± 0.1	–
476	0.9 ± 0.1	1.0 ± 0.2	1.2 ± 0.1	–
488	1.2 ± 0.1	1.2 ± 0.2	1.4 ± 0.1	–
496	1.5 ± 0.1	1.7 ± 0.3	–	–
501	2.0 ± 0.2	–	2.1 ± 0.1	–
514	3.4 ± 0.3	3.4 ± 0.2	3.8 ± 0.2	–
528	3.6 ± 0.4	–	–	–

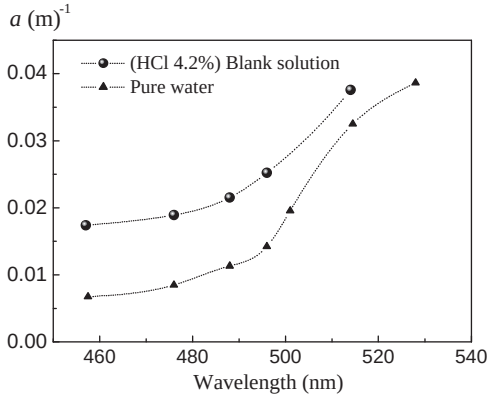

Fig. 14. Absorption spectra for the blank solution (HCl 4.2%) and pure water, obtained by the OMM configuration with a 100-mm cell length.

The OMM configuration is particularly important when high sensitivity is required. As an example, OMM was applied to measure the absorption spectrum of the 25-mg L^{-1} Cr(III) sample at nine excitation wavelengths (364, 457, 476, 488, 496, 501, 514, 594 and 632 nm). The result ($\theta/P_e l$) is shown also in Fig. 13 (right axis), and corresponds to the same spectrum shape obtained by the spectrophotometer (left axis). Except at 457 and 514 nm, where the available excitation power was high enough, the CMM configuration could not measure this spectrum due to the short cell length (2 mm).

Since the HCl and Cr(III) concentrations in the samples are relatively low, sample's parameters such as thermal conductivity (k) and temperature coefficient of refractive index (dn/dT) are expected to be close to the water's. The blank solution (HCl 4.2%) has thermal conductivity $k = 0.57$ W/m K [42], close to the water's value, 0.60 W/m K [33]. Moreover, fits of transient TL signals of the Cr(III) solutions provided the same thermal diffusivity found in pure water. Thus, we could calculate the absorption coefficient of the samples by Eq. (4), using Fig. 12's result and the data $k = 0.57$ W/m K and $dn/dT = -9.8 \times 10^{-5}$ K^{-1} (of water) [33]. The absorptivity of the solution, defined as the absorbance ($A = 0.434al$) normalized by the concentration (c) and the cell length (l), also was determined. At 514 nm, we found $A/cl \cong 8.1 \times 10^{-5}$ $(\text{mg L}^{-1}\,\text{cm})^{-1}$, which means that for a 1 mg mL^{-1} sample in 1-cm cell, $A \cong 0.081$. This value agrees well with the absorption spectrum in Fig. 13, obtained by a spectrophotometer.

The LOD found by TL (40 ng mL^{-1}) at 514 nm corresponds to an absorbance of $\sim 3.2 \times 10^{-4}$ for a 1-m cell length. This value is ~30 times smaller than the LOD found by conventional transmission techniques ($A \sim 10^{-2}$, with $l \sim 1$ m) [28,29].

Fig. 14 compares the absorption spectra of the blank solution (HCl 4.2%) with pure water, obtained by the OMM configuration using a cell with a 100-mm length.

4. Conclusions

We have applied the optimized mode-mismatched (OMM) thermal lens (TL) configuration to the study of Cr(III) solutions, pure and tap waters in the range 335–632 nm. This TL configuration uses an expanded and collimated probe beam and a focused excitation beam, which corresponds to detect the TL in the near field condition. It has some interesting features: it allows the use of thick samples, which improves the sensitivity, and maximizes the signal, reaching its maximum theoretical value $S = \theta\pi/2$. This condition is independent of the Rayleigh beam parameters and relative positions of their beam waists, which simplifies the experiment calibration and improves the experiment accuracy. This simplification is particularly important when several lasers lines are used, like in this experiment. The TL signal was observed to increase linearly with sample length, varying l from 5 to 100 mm. Using a 100-mm cell, the detection limit was of 1×10^{-6} cm^{-1} with $P_e = 180$ mW at 364 nm for water. From this data we estimated a detection limit of $\sim 2 \times 10^{-7}$ cm^{-1} for $P_e = 1$ W for water, and $\sim 6 \times 10^{-9}$ cm^{-1} for CCl_4, which is usually considered as a good solvent for photothermal measurements of low absorption. Therefore, we demonstrated that very high sensitivity can be obtained using the OMM approach even using a solvent with very low photothermal enhancement factor (E) like water, which has $E \sim 33$ times smaller than CCl_4. For Cr(III) species in HCl (4.2%) aqueous solution, the limit of detection (LOD) was ~40 ng mL^{-1} at 514 nm, or ~10 ng mL^{-1} at 405 nm, which is ~30 times smaller than the LOD achieved with conventional transmission techniques. Considering the experimental uncertainty, results of the conventional dual-beam TL configuration (used where absorption was high enough) corroborated the results obtained in the OMM TL setup. As drawbacks of OMM, it requires longer acquisition times and smaller aperture because the lens effect is more concentrated in the center of the probe beam, as a consequence of the near field condition.

Acknowledgements

This research was supported by Brazilian agencies FAPESP (Fundação de Amparo à Pesquisa do Estado de São Paulo), CAPES (Coordenação de Aperfeiçoamento de Pessoal de Nível Superior), CNPq (Conselho Nacional de Desenvolvimento Científico e Tecnológico) and FAPERJ (Fundação de Amparo à Pesquisa do Estado do Rio de Janeiro). The authors are also thankful to Dr. Francisco E. G. Guimarães and Dr. Máximo S. Li for allowing the use of the He–Cd and Kr^+ lasers.

References

[1] J. Georges, Spectrochim. Acta A 69 (2008) 1063.
[2] M.A. Proskurnin, E.V. Ageeva, V.V. Senyuta, N.V. Orlova, A.V. Fokin, O.B. Ovchinnikov, S.V. Egerev, Talanta 81 (2010) 377.
[3] M.A. Proskurnin, M.Y. Kononets, Usp. Khim. 73 (2004) 1235.
[4] M. Franko, Talanta 54 (2001) 1.
[5] S.E. Bialkowski, Photothermal Spectroscopy Methods for Chemical Analysis, John Wiley & Sons, Inc., New York, 1996.
[6] R.D. Snook, R.D. Lowe, Analyst 120 (1995) 2051.
[7] H.L. Fang, R.L. Swofford, In: Kliger (Eds.), Ultrasensitive Laser Spectroscopy, Academic Press, New York, 1983, pp. 204.
[8] M.L. Baesso, J. Shen, R.D. Snook, J. Appl. Phys. 75 (1994) 3732.
[9] C.D. Tran, S. Challa, M. Franko, Anal. Chem. 77 (2005) 7442.
[10] P.R.B. Pedreira, L.R. Hirsch, J.R.D. Pereira, A.N. Medina, A.C. Bento, M.L. Baesso, M.C.E. Rollemberg, M. Franko, Chem. Phys. Lett. 396 (2004) 221.
[11] C.K.N. Patel, A.C. Tam, Nature 280 (1979) 302.
[12] F.M. Sogandares, E.S. Fry, Appl. Opt. 36 (1997) 8699.
[13] M. Hass, J.W. Davisson, J. Opt. Soc. Am. 67 (1977) 622.
[14] S.J. Sheldon, L.V. Knight, J.M. Thorne, Appl. Opt. 21 (1982) 1663.
[15] S.M. Lima, J.A. Sampaio, T. Catunda, A.C. Bento, L.C.M. Miranda, M.L. Baesso, J. Non-Cryst. Solids 273 (2000) 215.
[16] T. Berthoud, N. Delorme, P. Mauchien, Anal. Chem. 57 (1985) 1216.
[17] J. Shen, R.D. Lowe, R.D. Snook, Chem. Phys. 165 (1992) 385.
[18] A. Marcano, H. Cabrera, M. Guerra, R.A. Cruz, C. Jacinto, T. Catunda, J. Opt. Soc. Am. B 23 (2006) 1408.
[19] H. Cabrera, A. Marcano, Y. Castellanos, Condens. Matter Phys. 9 (2006) 385.
[20] R.A. Cruz, A. Marcano, C. Jacinto, T. Catunda, Opt. Lett. 34 (2009) 1882.
[21] N.J. Dovichi, J.M. Harris, Anal. Chem. 53 (1981) 106.
[22] R.M. Pope, E.S. Fry, Appl. Opt. 36 (1997) 8710.
[23] H. Buiteveld, J.H.M. Hakvoort, M. Donze, In: J.S. Jaffe, SPIE Proceedings on Ocean Optics XII, SPIE - Int Soc Optical Engineering, 1994, pp. 174.
[24] R.C. Smith, K.S. Baker, Appl. Opt. 20 (1981) 177.
[25] T.I. Quickenden, C.G. Freeman, R.A.J. Litjens, Appl. Opt. 39 (2000) 2740.
[26] E.S. Fry, Appl. Opt. 39 (2000) 5843.
[27] A. Morel, B. Gentili, H. Claustre, M. Babin, A. Bricaud, J. Ras, F. Tieche, Limnol. Oceanogr. 52 (2007) 217.
[28] L.P. Boivin, W.F. Davidson, R.S. Storey, D. Sinclair, E.D. Earle, Appl. Opt. 25 (1986) 877.
[29] R.A.J. Litjens, T.I. Quickenden, C.G. Freeman, Appl. Opt. 38 (1999) 1216.
[30] M. Sikovec, M. Novic, V. Hudnik, M. Franko, J. Chromatogr. A 706 (1995) 121.
[31] N.J. Dovichi, J.M. Harris, Anal. Chem. 51 (1979) 728.

[32] J. Shen, A.J. Soroka, R.D. Snook, J. Appl. Phys. 78 (1995) 700.
[33] D.N. Nikogosyan, Properties of Optical and Laser Related Materials: A Handbook, John Wiley & Sons, New York, 1997.
[34] P.R.B. Pedreira, L. Hirsch, J.R.D. Pereira, A.N. Medina, A.C. Bento, M.L. Baesso, Rev. Sci. Instrum. 74 (2003) 808.
[35] J. Shen, M.L. Baesso, R.D. Snook, J. Appl. Phys. 75 (1994) 3738.
[36] C. Jacinto, D.N. Messias, A.A. Andrade, S.M. Lima, M.L. Baesso, T. Catunda, J. Non-Cryst. Solids 352 (2006) 3582.
[37] J.S. Bartlett, K.J. Voss, S. Sathyendranath, A. Vodacek, Appl. Opt. 37 (1998) 3324.
[38] J.B. Thorne, D.R. Bobbitt, Appl. Spectrosc. 47 (1993) 360.
[39] M. Costa, Crit. Rev. Toxicol. 27 (1997) 431.
[40] J. Barcelo, C. Poschenrieder, B. Gunse, J. Exp. Bot. 37 (1986) 178.
[41] E. Otabbong, Acta. Agric. Scand. 39 (1989) 149.
[42] Solvay, Hydrochloric Acid http://www.solvaychlorinatedinorganics.com/library/bysection/result/0,0,-_EN-1000024,00.html. May 21, 2008.